CHAPTER 4

ATTENUATION COEFFICIENTS OF CARBON STEEL PLATES

4.1   Introduction

Study of the fundamental of radiation interactions with matter has become an important research area in NDT. The data on the attenuation of gamma rays and X-rays in material is required for many scientific, engineering and medical applications. An example of an application for attenuation coefficient measurement in biological studies is the measurement of linear attenuation coefficient for Rhizophora spp. wood. [35]. The density of the material is very close to water which is 1.029 ± 0.006 g/cm^3 and in view of this, the energy used must be low energy, 11.22 to 28.43 keV. Gamma ray attenuation coefficients of building materials were also studied [7]. Singh et. al [36] studied the gamma attenuation of PbO-BaO-B$_2$O$_3$ glass system which is used in radiation shielding. The photon energies used in this experiment were 511, 662 and 1274 keV. In his work, the attenuation coefficients of the materials were measured in narrow beam transmission geometry. The results show that the mass attenuation coefficients increase linearly with the increase of the lead weight fraction in the material. Akkurt [8] also studied the photon attenuation coefficients in concrete which is used for radiation shielding. Gurdeep et. al [37,38] have measured the mass attenuation coefficient on different media namely bakelite, perspex, soil and water using 662 keV gamma ray. They also studied the effect of collimator size and the absorber thickness on gamma ray. Dorobantu [39] studied the linear attenuation coefficient of X-ray in steel with thickness dependance. Akkurt [40] studied the effective atomic and electron numbers in different steels at different energies. His study shows that the linear

attenuation coefficient for a material depends on the incident photon energy, the effective atomic number and the density of the material. Susan [41] measured the gamma ray mass attenuation coefficients for industrial materials such as n-pentane, ethanol, toluene, olein, oil sludge, polyethylene, distilled water, cement, brick and concrete using 356 keV and 662 keV gamma ray.

This chapter discusses the experimental procedure to investigate the effect of the attenuation coefficient of carbon steel using film radiography and ion chamber detector when gamma radiation from radioisotope Iridium-192 interacts with thin carbon steel plates. The methodology of the experiments is explained and the results are analysed in this chapter. However, for ion chamber detector, two experiments are carried out. The first experiment uses narrow beam where the initial beam is collimated using a lead collimator. In the second experiment, the beam used is a broad beam which is not collimated with any collimator. The attenuated intensity and attenuation coefficients are shown and discussed.

4.2   Sample Preparation

The billet sample shown in Figure 4.1 is supplied by Southern Steel Berhad, Perai, Pulau Pinang. It is made from carbon steel with dimensions 141 mm × 141 mm × 98 mm composing of various elements such as iron (Fe), carbon (C), silicon (Si), manganese (Mn), phosphorus (P), sulphur (S), copper (Cu), nickel (Ni), chromium (Cr), aluminium (Al), calcium (Ca), molybdenum (Mo), tin (Sn) and nitrogen (N).

Figure 4.1 The billet.

The percentage of each element in the sample is shown in Table 4.1. It can be seen that iron has the highest fraction in the sample which amounts to 98.5% of the composition while other elements contribute to the remaining 1.5% of the elements in the sample. Since the percentage of iron is large, iron is expected to have the dominant cross section in this sample.

Table 4.1 Composition of the carbon steel sample.

Element	Percentage (%)
Fe	98.5108
C	0.21
Si	0.19
Mn	0.59
P	0.013
S	0.029
Cu	0.250
Ni	0.08
Cr	0.08
Al	0.0018
Ca	0.0007
Mo	0.016
Sn	0.02
N_2	0.0087

The sample is grinded using the grinding machine shown in Figure 4.2 to obtain the specific dimensions. The sample is then cut according to various specified thickness with tolerance of +0.5 to 1 mm and achive the uniform thickness to a region of 70%-85%. The range of thickness chosen for this experiment is listed in Table 4.2. The samples according to the thickness in Table 4.2 are obtained and classified as thin carbon steel plates. Akkurt [8] used thin concrete samples in his experiments. Since concrete and steel are dense materials, we aspect the behaviour of the attenuation in this samples to be similar.

Figure 4.2 Grinding process.

Table 4.2 The thickness of the plates used in the experiment.

Thickness (mm)	2.0	3.0	5.0	6.8	11.1	13.0

After the billet has been cut into plates with its required thickness (Figure 4.3), the final step is to put the plates on the polishing machine in order to obtain a smooth surface as shown in Figure 4.4.

Figure 4.3 Cutting process.

Figure 4.4 Polishing process.

4.3 Film Radiography Experiments

4.3.1 Film as the Detector

The radiation source used in this experiment is Iridium-192. The radiation output for Iridium-192 is 0.5 $RhmCi^{-1}$ at one metre [19]. The exposure of the Iridium-192 used is 2.4 Cihr. The source to film distance (SFD) is 100 cm. Lead screens with thickness 0.125 mm are placed at the front and back of the film. D7 films are used in this experiment. Figure 4.5 depicts the set-up of the experiment. The beam is narrow collimated by adjusting the collimator at the source. Fog density which is the density

registered by the film without any radiation source it is due to background radiation from the environment to the film, is measured first before using the plates. Likewise unabsorbed radiation density D_0 which refers to the density from the source without passing any material is also determine before starting the experiment. The plate thickness of 6.8 mm is used as the reference thickness to determine the exposure time for the other plates. The exposure is determine from the exposure chart for steel [42]. The density of the exposed film at this thickness is in the range 2.0-2.5. The range of density is refered to as the measured film density. An average of three measurements at three locations are made; one at the centre and two at opposite sides of the centre point on each plate. Film density of the exposed films D is then the difference between the measured film density and the fog density.

The density of the radiated film, D is propotional to the intensity of the radiation after passing through the sample. Thus, D ought to have the same behaviour as for intensity i.e. $D \sim I$. In this way, the film density has a decay profile [39] similar to the Beer's Lambert Law in Equation (2.1):

$$D = D_0 e^{-\mu t} . \qquad (4.1)$$

Plotting $ln(D/D_0)$ versus thickness t would give a linear relationship with decreasing slope:

$$ln(D/D_0) = -\mu t \qquad (4.2)$$

whereby the gradient gives the attenuation coefficient of carbon steel for each thickness:

$$\mu = -ln(D/D_0)/t . \qquad (4.3)$$

The variation of film density sample with plate thickness is given in Table 4.3 and Figure 4.6 while Table 4.4 and Figure 4.7 show the attenuation coefficient of each plate calculated using Equation (4.3).
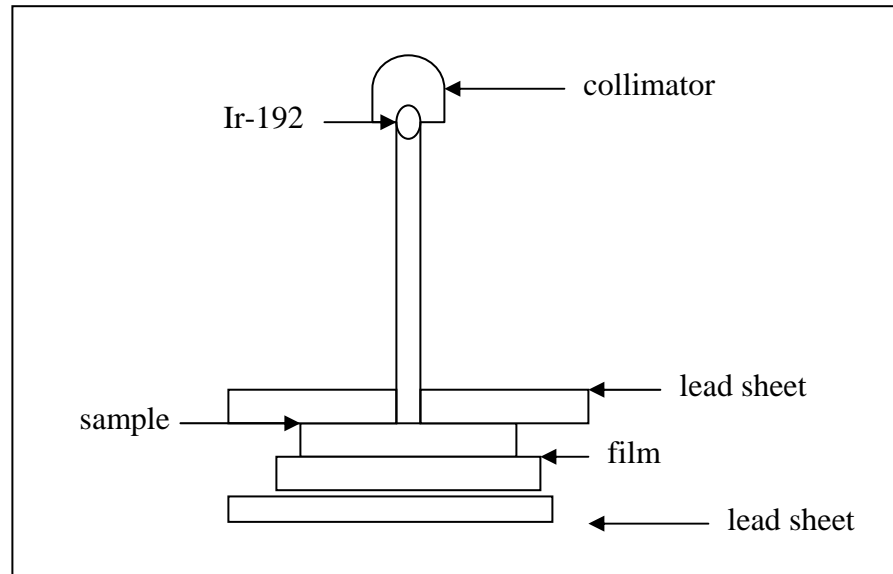

Figure 4.5 Film radiography: narrow collimated beam method.

4.3.2 Film as the Detector with highly Collimated Beam

In the second experiment, we have taken some precautions to minimise errors: the opening of the collimator is measured at 14.4 mm. In the first experiment, the opening of the collimator was not taken into consideration. The film density is measured at three equidistance points with respect to the centre of the film but the range is kept equal to the opening of the collimator. In this way, we essentially measure a highly collimated ray and thus avoiding diverging rays. The target film density is still in the range of 2.0 to 2.5 at plate thickness 6.8 mm. The result of the second experiment is given in Table 4.5 and Figure 4.8. The attenuation coefficient is shown in Table 4.6 and Figure 4.9.

4.3.3 Result and Discussion

1. First experiment : film as the detector

   Unabsorbed radiation density $D_0 = 3.43 \ (1 \pm 0.03)$

   Fog density $= 0.29 \ (1 \pm 0.03)$

Table 4.3. Film radiography: density as a function of thickness for the first experiment.

Thickness (mm)	Measured Film Density	Film Density, D (measured film density – fog density)
2.0	2.43 (1 ± 0.03)	2.14 (1 ± 0.03)
3.0	2.34 (1 ± 0.03)	2.05 (1 ± 0.03)
5.0	2.38 (1 ± 0.03)	2.09 (1 ± 0.03)
6.8	2.15 (1 ± 0.03)	1.86 (1 ± 0.03)
11.1	1.85 (1 ± 0.03)	1.56 (1 ± 0.03)
13.0	1.81 (1 ± 0.03)	1.52 (1 ± 0.03)

Table 4.4. Film radiography: attenuation coefficient for various thicknesses for the first experiment.

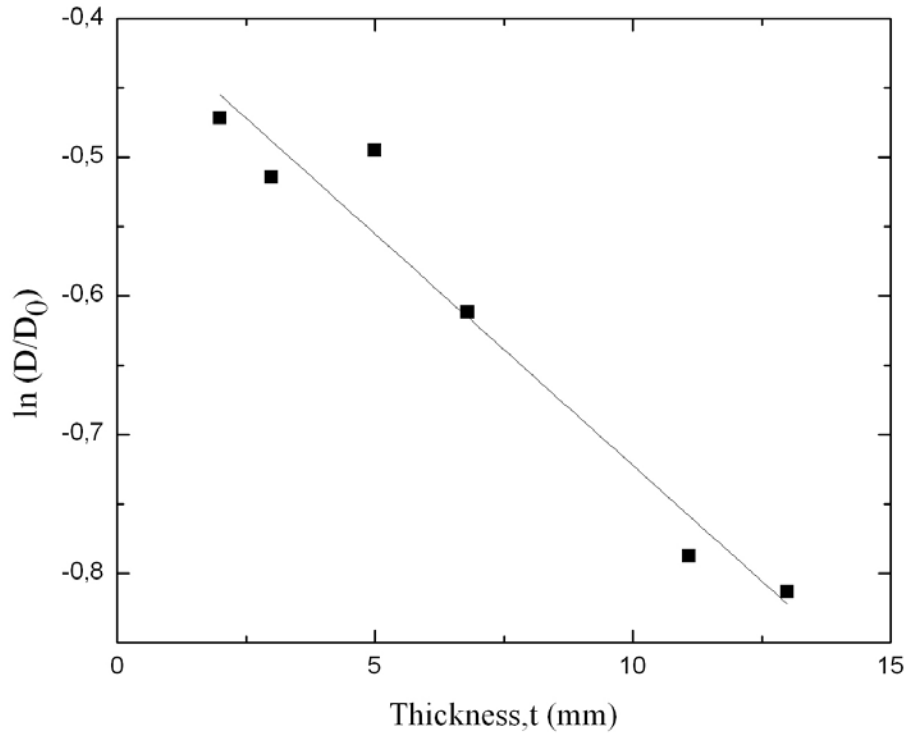| Thickness (mm)	Film Density, D (measured film density – fog density)	Attenuation Coefficient, μ $\left(\text{cm}^{-1}\right)$
2.0	2.14 (1 ± 0.03)	2.36
3.0	2.05 (1 ± 0.03)	1.72
5.0	2.09 (1 ± 0.03)	0.99
6.8	1.86 (1 ± 0.03)	0.87
11.1	1.56 (1 ± 0.03)	0.72
13.0	1.52 (1 ± 0.03)	0.63

Figure 4.6 Film radiography: film density versus thickness for the first experiment.

Figure 4.6 shows the film density as a function of plate thickness for the first experiment using film radiography as given in Table 4.3. From the graph, as the thickness of the plate increases the density of the film decreases. This phenomena is due to the attenuation process that happens in the material when the photons interact with the sample. However, in this process, the pair production process is not involve due to the energy of the photons being less than the energy of photons for pair production. Hence, only two dominant processes are involved which are photoelectric absorption and incoherent scattering processes.
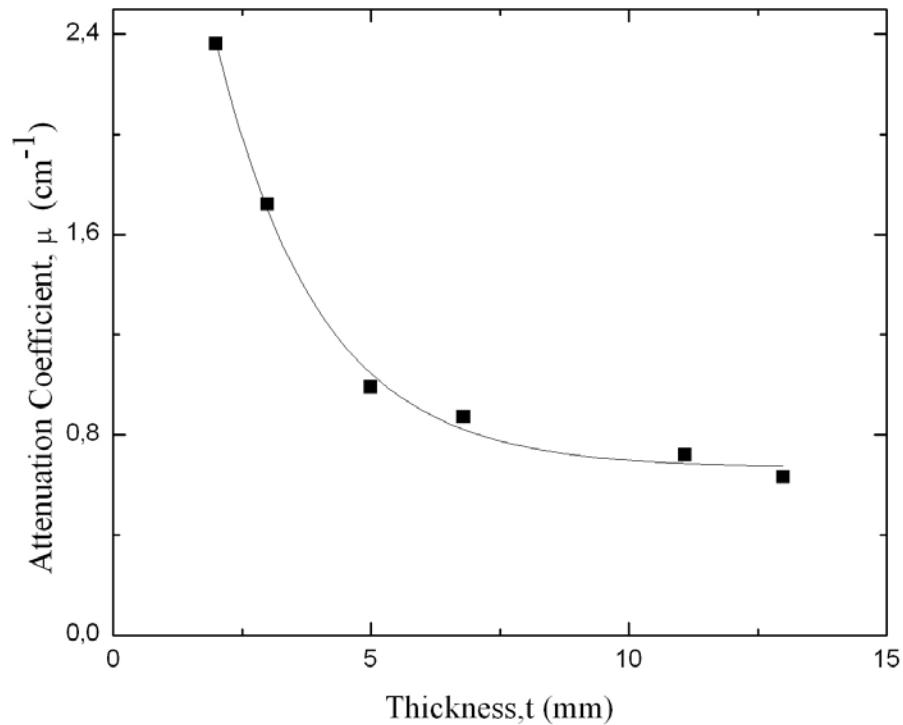
Figure 4.7 Film radiography: attenuation coefficient versus thickness of samples for the first experiment.

Figure 4.7 shows the attenuation coefficient for film detectors with different thickness of the carbon steel plates. The attenuation decreases exponentially as the thickness of samples increases.

2. Second experiment: film as the detector with diameter of the opening of the collimator at 14.4 mm.

Unabsorbed radiation density = 3.21 (1 ± 0.03)

Fog density = 0.23 (1 ± 0.03)

Table 4.5. Film radiography: density as a function of thickness for the second experiment.

Thickness (mm)	Measured Film Density	Film Density, D (measured film density – fog density)
2.0	2.79 (1 ± 0.03)	2.56 (1 ± 0.03)
3.0	2.73 (1 ± 0.03)	2.50 (1 ± 0.03)
5.0	2.58 (1 ± 0.03)	2.35 (1 ± 0.03)
6.8	2.31 (1 ± 0.03)	2.08 (1 ± 0.03)
11.1	2.11 (1 ± 0.03)	1.88 (1 ± 0.03)
13.0	1.96 (1 ± 0.03)	1.73 (1 ± 0.03)

Table 4.6. Film radiography: attenuation coefficient for various thicknesses for the second experiment.

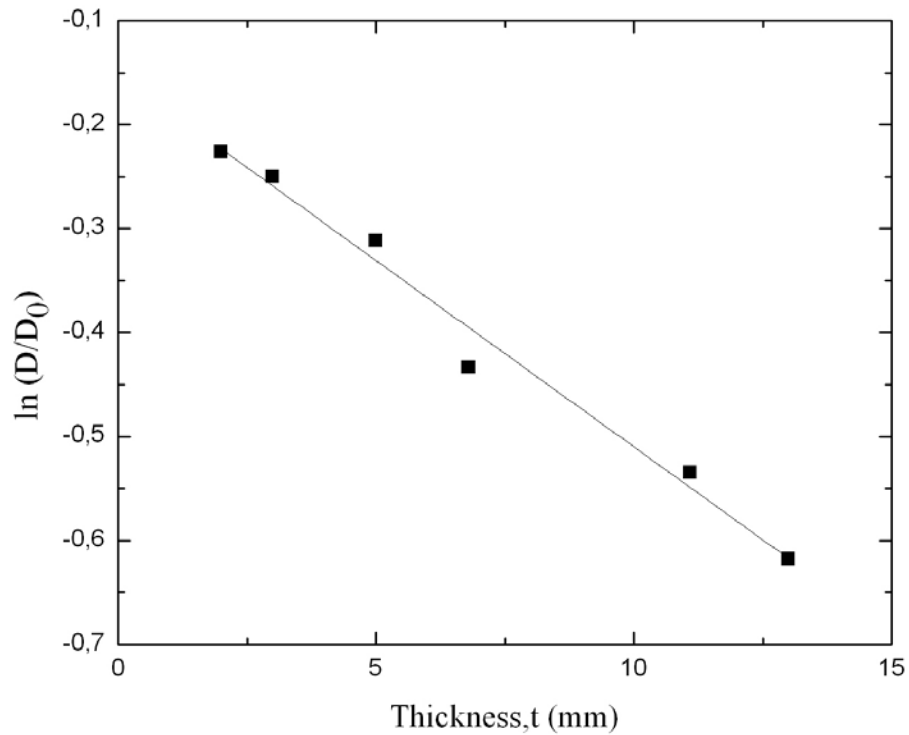| Thickness (mm)	Film Density, D (measured density – fog density)	Attenuation Coefficient, μ $\left(\text{cm}^{-1}\right)$
2.0	2.56 (1 ± 0.03)	1.13
3.0	2.50 (1 ± 0.03)	0.83
5.0	2.35 (1 ± 0.03)	0.62
6.8	2.08 (1 ± 0.03)	0.62
11.1	1.88 (1 ± 0.03)	0.49
13.0	1.73 (1 ± 0.03)	0.48

Figure 4.8. Film radiography: density versus thickness for the second experiment.

Figure 4.8 shows the film density as a function of plate thickness for film detectors in the second experiment. The graph shows that as the thickness increases the density of the film decreases even though in this setting the radiation is highly collimated. Figure 4.8 shows the same trend as in Figure 4.6.
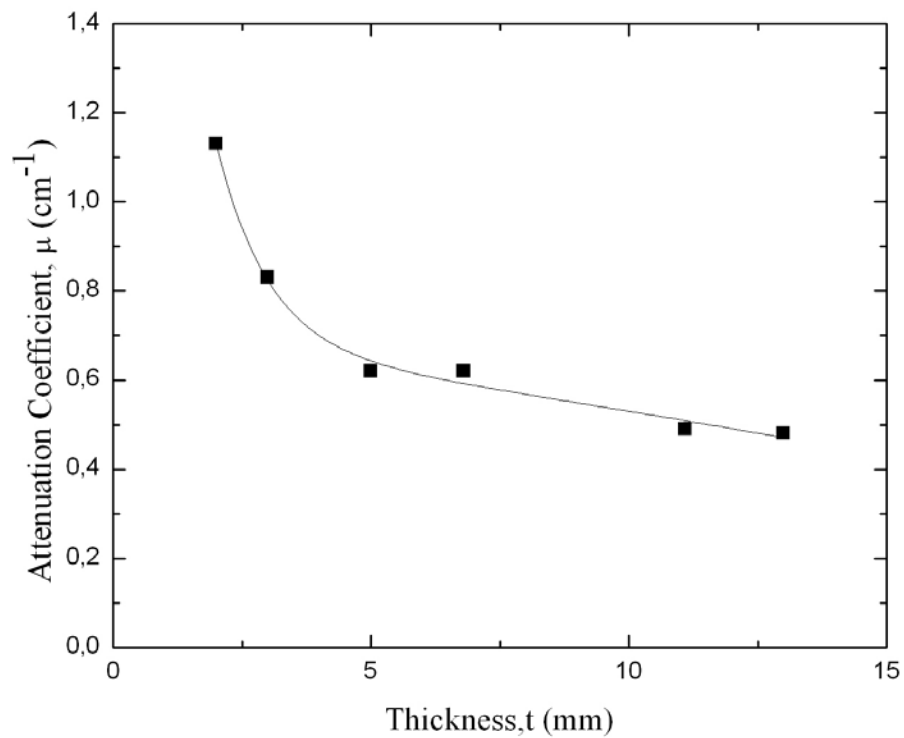
Figure 4.9. Film radiography: attenuation versus thickness for the second experiment.

Figure 4.9 shows the attenuation for film detectors with different thickness using highly collimated beam in the second experiment. The graph exhibit the same trend as in Figure 4.7 in that it attenuates exponentially as the thickness of samples increases.

4.4   Ion Chamber Experiments

4.4.1   Collimated Beam Condition

In order to check the consistency of our radiography experiments, a third experiment with different detector is used. The detector used in this experiment is a Radcal Corporation radiation monitor controller, model 2026c with sensor 20×6-180 cc ion chamber. The minimum dose rate for this sensor is 1 mR/hr and the maximum dose rate detection is 1 kR/hr. The resolution of the detector is 1 mR/hr. The energy dependance of the ion chamber is $\pm 5\%$, 30 keV to 1.33 MeV with build up material. Intensity from the source I_0 and the attentuated intensity I are measured. From Equation (2.1), the intensity is plotted according to the following linear equation:

$$\ln(I/I_0) = -\mu t \tag{4.4}$$

and consequently the attenuation coefficient is calculated using

$$\mu = -ln(I/I_0)/t . \tag{4.5}$$

The results of the experiment are shown in Table 4.7, Table 4.8, Figure 4.10, Figure 4.11, Figure 4.12 and Figure 4.13.

4.4.2   Broad Beam Condition

In the fourth experiment, the rays are not collimated with a lead collimator. The rays are in broad beam condition. The purpose of this experiment is to study the behaviour of the attenuation curve when broad beam is used instead of narrow collimated beam. The detector used in the fourth experiment is the ion chamber as described in Section 4.4.1. Intensity from the source I_0 and the attenuated intensity I

are measured. The results are shown in Table 4.9, Table 4.10, Figure 4.14 and Figure 4.15.

4.4.3 Result and Discussion

3. Third experiment: ion chamber as the detector with collimated beam

Background intensity = 0 mR/hr

Unabsorbed intensity, I_0 = 12.14 mR/hr

Table 4.7. Ion chamber: density as a function of thickness for the third experiment.

Thickness (mm)	Measured Intensity (mR/hr)	Intensity, I (measured intensity – background intensity)
2.0	8.17	8.17
3.0	7.59	7.59
5.0	7.24	7.24
6.8	7.12	7.12
11.1	5.95	5.95
13.0	5.60	5.60

Table 4.8. Ion chamber: attenuation coefficient with various thicknesses for the third experiment.

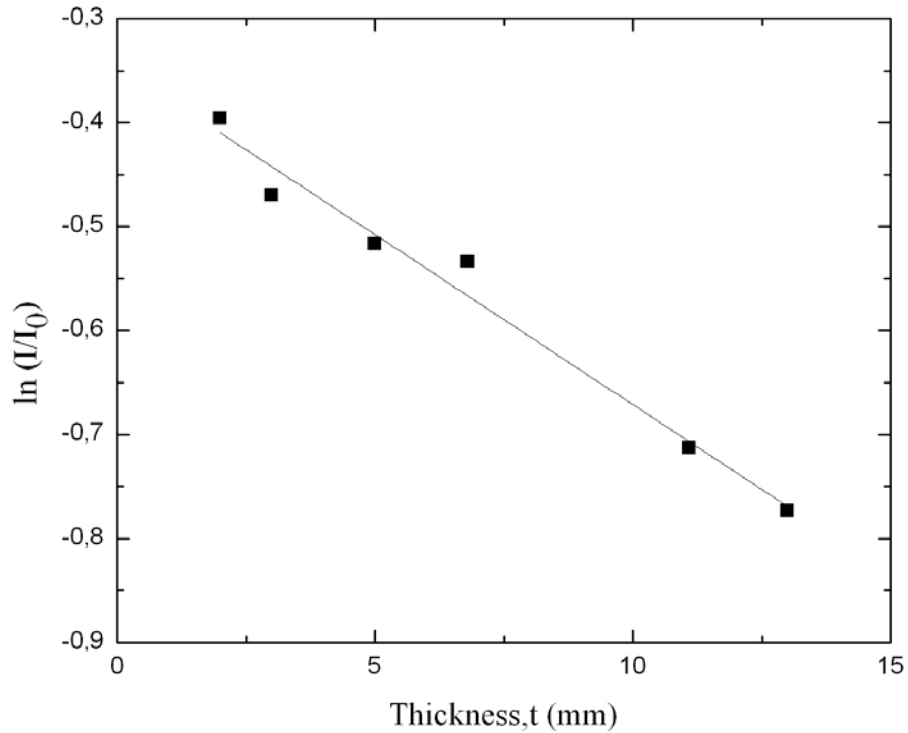| Thickness (mm)	Intensity, I (measured intensity – background intensity)	Attenuation Coefficient, μ (cm^{-1})
2.0	8.17	1.98
3.0	7.59	1.57
5.0	7.24	1.03
6.8	7.12	0.76
11.1	5.95	0.65
13.0	5.60	0.60

Figure 4.10 Ion chamber: intensity versus thickness for the third experiment.

Figure 4.10 shows the intensity curve as a function of plate thickness using ion chamber as the detector with narrow beam. From the graph, we can see that the intensity decreases when the thickness of the samples is increased. The decreasing of intensity when the thickness of sample is increased is due to the attenuation process when the photons are passing through the sample.
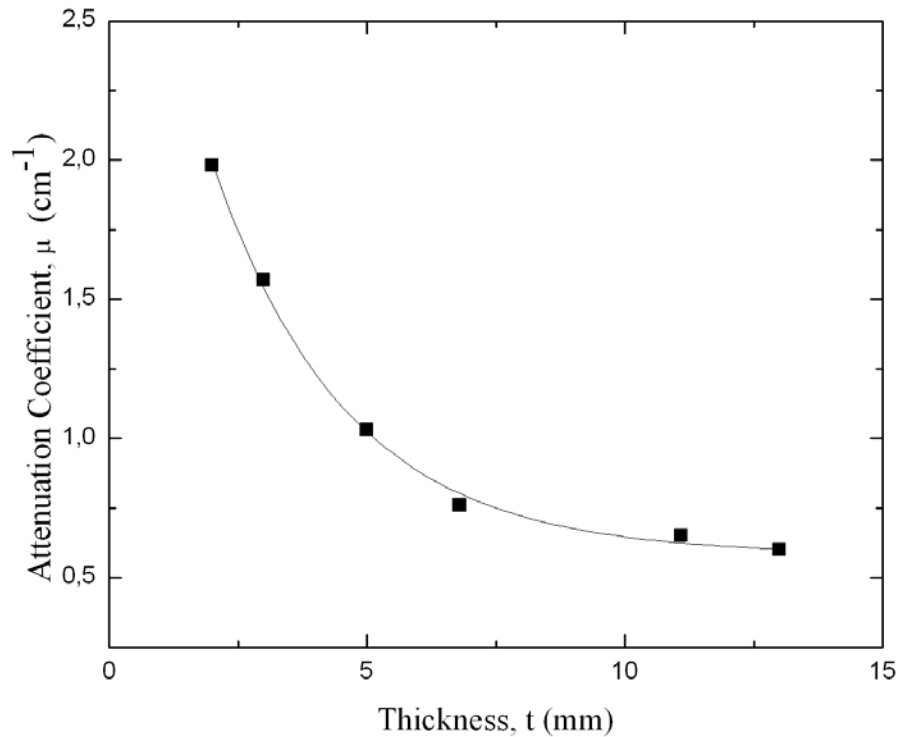
Figure 4.11. Ion chamber: attenuation coefficient versus thickness for the third experiment.

The attenuation curve which is shown in Figure 4.11 obeys the attenuation law that is given in Equation (2.1). The attenuation curve drops exponentially as the thickness sample increases. The result obtained in this experiement also shows consistency with Shirakawa [43] where at thickness 11 mm, our results for ion chamber is 0.65cm^{-1} while Shirakawa's is 0.598 cm^{-1}.

4. Fourth experiment: ion chamber as the detector with broad beam (without collimator)

   Background intensity = 0 mR/hr

   Unabsorbed intensity, I_0 = 11.83 mR/hr

Table 4.9. Ion chamber: intensity as a function of thickness for the fourth experiment.

Thickness (mm)	Measured Intensity (mR/hr)	Intensity, I (measured intensity – background intensity)
2.0	11.11	11.11
3.0	10.76	10.76
5.0	10.07	10.07
6.8	9.38	9.38
11.1	8.02	8.02
13.0	7.40	7.40

Table 4.10. Ion chamber: attenuation coefficient with various thicknesses for the fourth experiment.

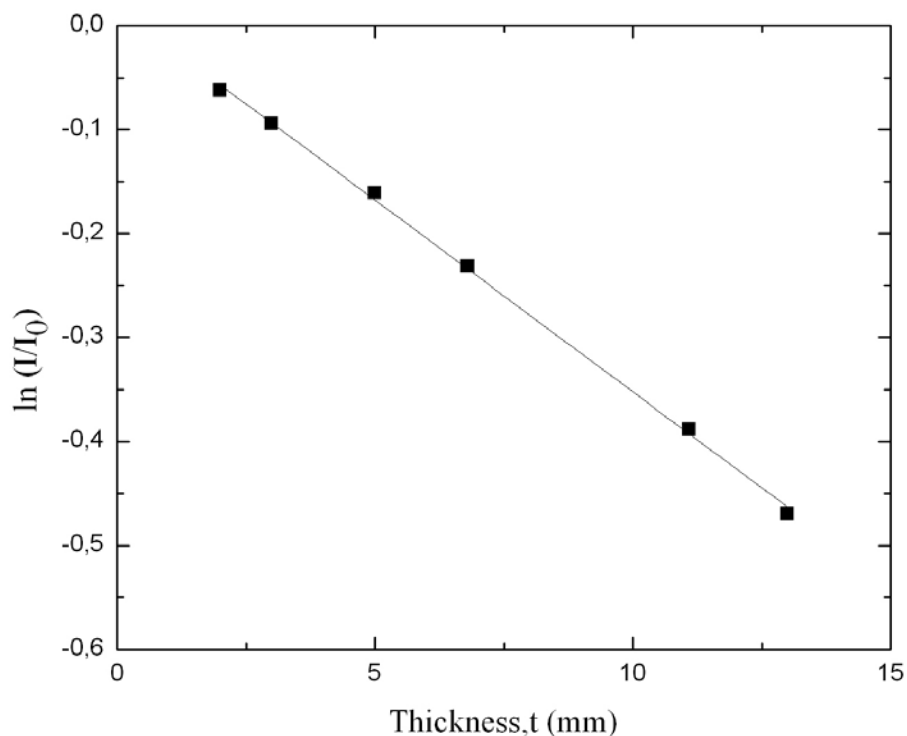| Thickness (mm)	Intensity, I (measured intensity – background intensity)	Attenuation Coefficient, μ (cm^{-1})
2.0	11.11	0.31
3.0	10.76	0.32
5.0	10.07	0.32
6.8	9.38	0.33
11.1	8.02	0.35
13.0	7.40	0.36

Figure 4.12 Ion chambers: intensity versus thickness for the fourth experiment.

Figure 4.12 shows the behaviour of the intensity when the plate thickness increases for the broad beam experiment. The graph shows expected behaviour of the intensity i.e. the intensity decreases when the thickness of the plates increases. This is due to the intensity being attenuated when passing through the material. The thicker the material, the more the intensity being attenuated. We note that there is a marked increased in the intensity recorded by approximately 50% than in the intensity of collimated beam experiments. This may be due to external scatterings, such as scatterings from the walls, ceiling and surrounding area that may affect the result. When non collimated beam is used, the probability of multiple scattered photons reaching the detector will increase.
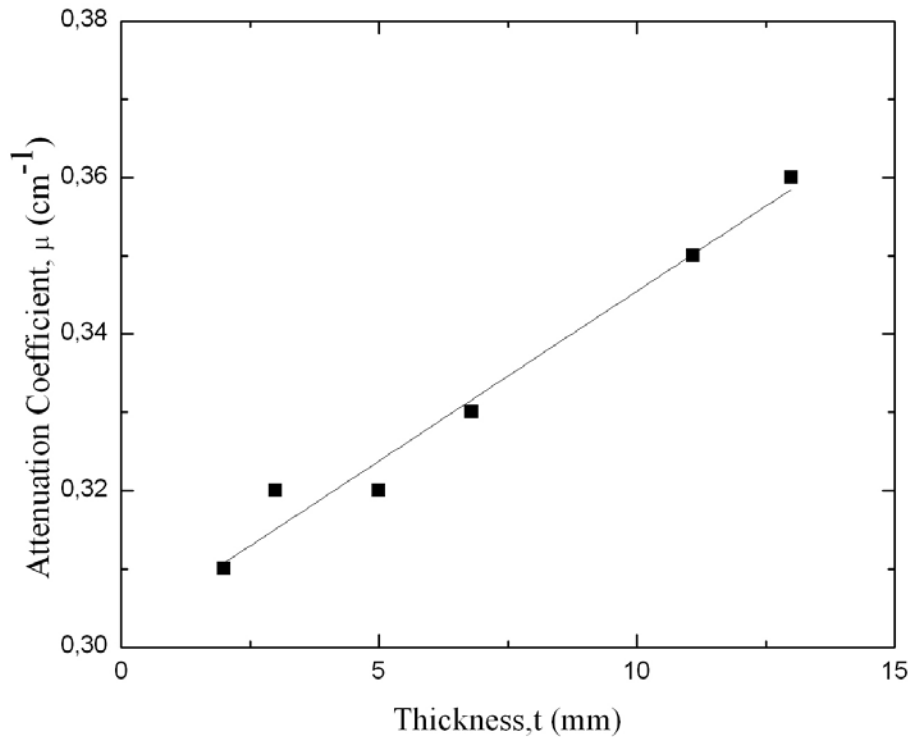
Figure 4.13 Ion chamber: attenuation coefficient versus thickness for the fourth experiment.

When non collimated beam is used as shown in Figure 4.13, the probability of multiple scattered photons reaching the detector will increase. This result agrees with Gurdeep et. al [37,38] which shows that the attenuation coefficient increases in sample thickness as well as with the size of collimator due to the contribution of external scatterings and multiple scatter photons in the uncollimated beam. Hence the attenuation curve does not follow the standard pattern.

4.5   Discussion

From the first and second experiments using film detector, the density values vary. When the density varies, the attenuation coefficient also varies between the two experiments. The difference between the first and second experiment using film is shown in Table 4.11.

Table 4.11. The difference in the attenuation coefficients for the film radiography experiments.

Thickness (mm)	$\mu\left(cm^{-1}\right)$ 1st experiment	$\mu\left(cm^{-1}\right)$ 2nd experiment	Difference in $\mu\left(cm^{-1}\right)$
2	2.36	1.13	1.23
3	1.72	0.83	0.89
5	0.99	0.62	0.37
7	0.87	0.62	0.25
11	0.72	0.49	0.23
13	0.63	0.48	0.15

From Table 4.11, the difference in the attenuation when using film as detectors shows a decrease in the attenuation values when the thickness of the samples starts to increase. This results show the same pattern in the work of Dorobantu [39]. At thickness 11.1 mm, the atteanuation coefficient obtained by Dorobantu [39] is 0.152 cm^{-1} and for this work the attenuation coefficient at 11.1 mm is higher which are 0.49 cm^{-1} for film and 0.65 cm^{-1} for the ion chamber detector. This is due to the source used in the experiment is different. Dorobantu exhibits lower attenuation coefficient because he used X-ray with energy 200 kV in his experiment. However, in this work Iridium-192 with higher energy from X-ray is used. Iridium-192 is a polychromatic radiations with different energies. Hence, this will decrease the values of attenuation coefficient when the thickness increases. This results agree with the theory proposed by Dorobantu

[39]. The results in this work also shows the same pattern as in Bochenin [44]. In his work, the thickness of steel used was in the range 1 to 5 mm of thickness and the sources were ^{90}Sr–^{90}Y radioactive nuclides. The sources used were low energy sources. For thin samples that are below 1 cm of thickness, extra care must be taken during the measurements. This is because any slight or small change in the measurement will result in much noticeble change in the intensity. Hence, it is recommended that for the experiment, the samples used must be more than 1 cm. The effective linear attenuation coefficient, μ used in Equation (2.1) is the average effect. It is non linear and has to be integrated over all energies.

The result for the first and second experiments as decribed earlier shows consistent results with the experiment done by Shirakawa [43]. In his experiment, at thickness 1 cm, attenuation coefficient is 0.595 cm^{-1} and for the second experiment done using film detector, the attenuation coefficient obtained is 0.51 cm^{-1}. While at 11 mm of thickness, the attenuation coefficient by Shirakawa is 0.598 cm^{-1} and from the second experiment using film, the value obtained is 0.49 cm^{-1}. Another factor that can affect the measurement is the type of films used which depends on the grain size.

The results, as shown in Figure 4.6, Figure 4.8, Figure 4.10 and Figure 4.12 are consistent with Shirakawa experiment [43]. The results exhibit a linear graph. Since the Iridium-192 is a heterochromatic beam, the output will be non linear graph[11]. However, the experiment setup is in highly collimated beam and good geometry condition as shown in Figure 4.5. Adding to this fact that the 0.316 MeV is the single most intense line in the spectrum, the behaviour of this radiation is not pronounce in the graphs.

However, the results in Figure 4.7, Figure 4.9 and Figure 4.11 do not show a linear graph but an exponential curve. The graph will become linear only when the monoenergetic beam is used but for heterochromatic beam like Iridium-192 attenuation coefficients will exhibit an exponential curve. The attenuation is dependant on energy lines in the radiation. Since Iridium-192 is a polychromatic beam, hence the attenuation coefficients are not constant.

Table 4.12. The attenuation coefficients for different detectors.

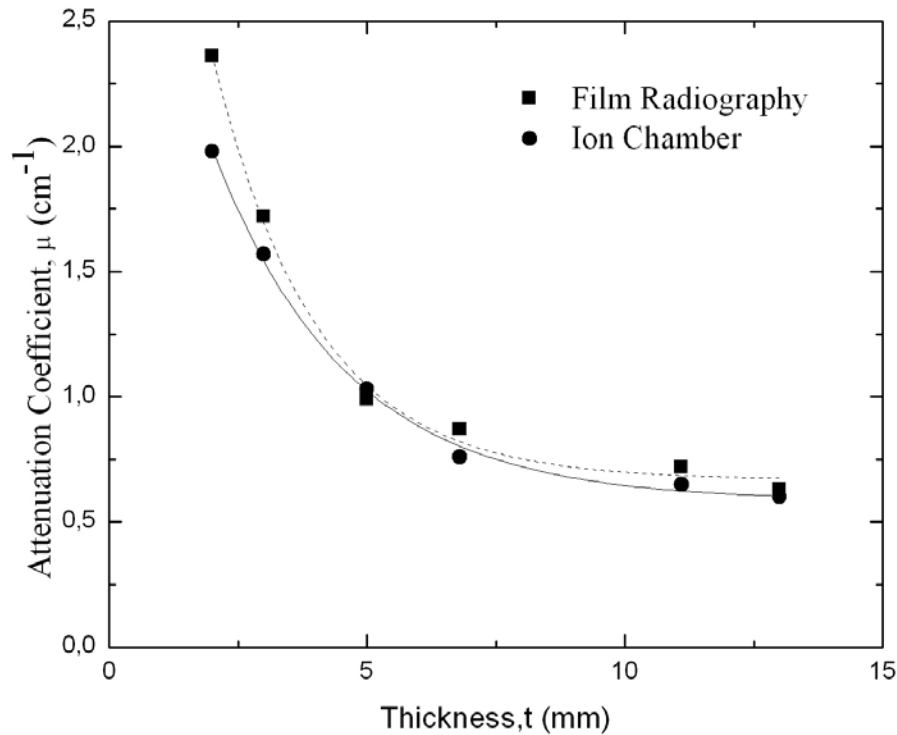| Thickness (mm)	$\mu \left(\text{cm}^{-1}\right)$ for film	$\mu \left(\text{cm}^{-1}\right)$ for ion chamber	Difference (%)
2.0	2.36	1.98	16.1
3.0	1.72	1.57	8.7
5.0	0.99	1.03	-4.0
6.8	0.87	0.76	12.6
11.1	0.72	0.65	9.7
13.0	0.63	0.60	4.8

Figure 4.14 Attenuation coefficient curves for different detectors.

The attenuation coefficients for the two different detectors used in this work i.e. the film detector and ion chamber are shown in Figure 4.14. The percentage difference in the attenuation coefficient for film detector and for ion chamber ranges from 16.1% to 4.0% as shown in Table 4.12. The highest difference is at thickness 2 mm and the lowest is at thickness 5.0 mm. The most important fact to emerge from this comparison is that the two experiments give consistent result. This serve a crucial verification of the accuracy of the experimental procedure.

The measurement of density in film radiography is affected by external factors. Those factors are human error involving film processing, external scattering, quality of film and grain size. In this experiments, the errors that exist are from many different sources. The densitometer that is used to measure the density can also be one of the

errors that affect the results. The errors from the densitometer is 3%. Another source of error is from the human error. The human error is very much related to the processing of the film. This happens especially at the agitation process of the film done by the operator during developing the film. The agitation process varies from each individuals which some might agitate harder and others might agitate softer. Another possible error is on the exposure time. The exposure time can be a little longer due to the retraction time. The retraction time of the source varies from each individual. The inaccurate exposure time can affect the density which finally affects the accuracy of the results.

The variations of grain size in films will also effect the results in the measurements. Thus, this is the limitation of using film for attenuation measurement. The grain density is defined as the number of grains per unit area of film. If the grain density is course, then the density obtained will be low and if the grain density is fine, then the density will be high. Hence, the definition of grain size is not meaningful. The grain size is inherent in the grain density, thus it is better to use the term grain density to discuss the physics in industrial radiography. The grain density, $\mathrm{grain}/\mathrm{cm}^2$, is in general not uniform throughout the surface of the film. In this experiment, all grains in the films must be fully processed. The density of the film will be less if the film is partially developed.

In our assumption, the film density is proportional to its intensity, $D \propto I$ [39]. However, in film radiography, the density of the film does not represent the actual intensity on the film. For example, for 100 grains in the film only 80 grains were irradiated which means that the actual density is not equivalent to the intensity. Thus, the proportionality constant is not unity but in actual fact is different for D_0 and D i.e. we propose that

$$D/D_0 = k_1 e^{-\mu t}/k_2 \tag{4.6}$$

and $k_1 \neq k_2$. The k_1 and k_2 are constants for the films and not from samples. From the above equation, $D \neq I$ and $D_0 \neq I_0$, and thus, the film density is not equal to the actual intensity impinging on the sample. The density of the film (grains) measured by the densitometer is only the grains that have been irradiated. The measured density is dependent on the grain density.

In this work, an experiment has been done with a broad beam using the ion chamber. However, the result obtain from this experiment is not consistent (Figure 4.13) with the analysis done when using narrow or collimated beam (Figure 4.11). Contrary to Halmshaw's [45] suggestion, broad beam is more suitable for qualitative work. The collimated beam is more reliable for quantitative, precision and measurement work. Halmshaw's suggestions are true if the source size is bigger than the sample and if the beam used is highly energetic and very broad. If these conditions are fulfilled, then the central part of the broad beam will almost be collimated.
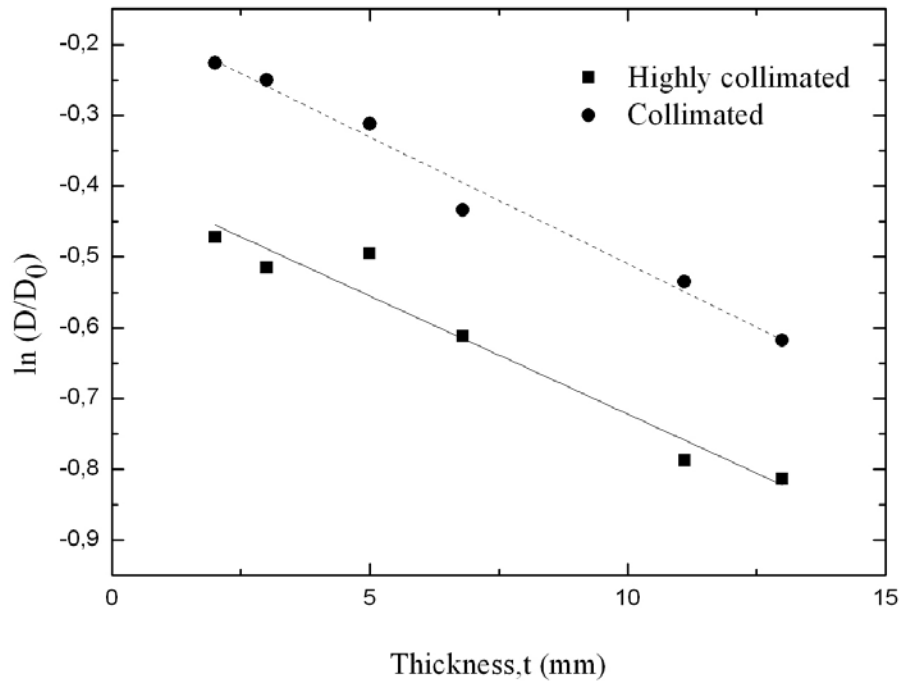
Figure 4.15 Comparison between the intensity in the collimated and highly collimated beam in the film radiography experiments.

Figure 4.15 shows the comparison between normal beam setup and highly collimated beam in the film radiography experiments. It can be seen that the film density of the highly collimated beam has lower registered density since the beam is narrower. This is consistent with the attentuation curves shown in Figure 4.16 where the highly collimated beam is less attenuated by the sample.
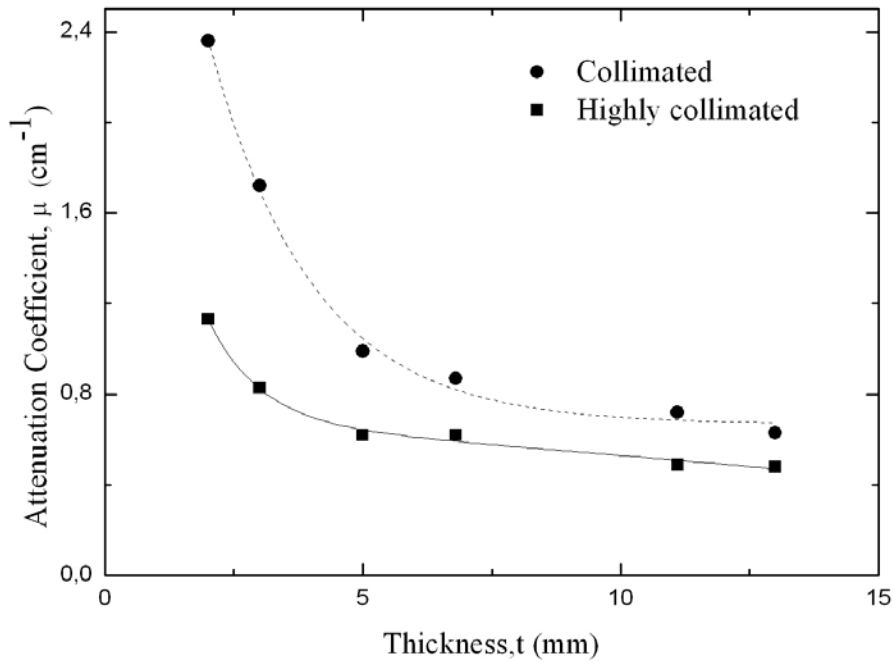
Figure 4.16 Comparison between the attenuation coefficient in the collimated and highly collimated beam in the film radiography experiments.

Broad beam experiment has a higher intensity registered by the ion beam detector compared with the narrow beam due to production of more secondary and scattered radiation as shown in Figure 4.17. The detector receives more photons than the detector with the narrow beam. It produces increasing attenuation coefficient with plate thickness in contrast with the narrow beam depicted by Figure 4.18.
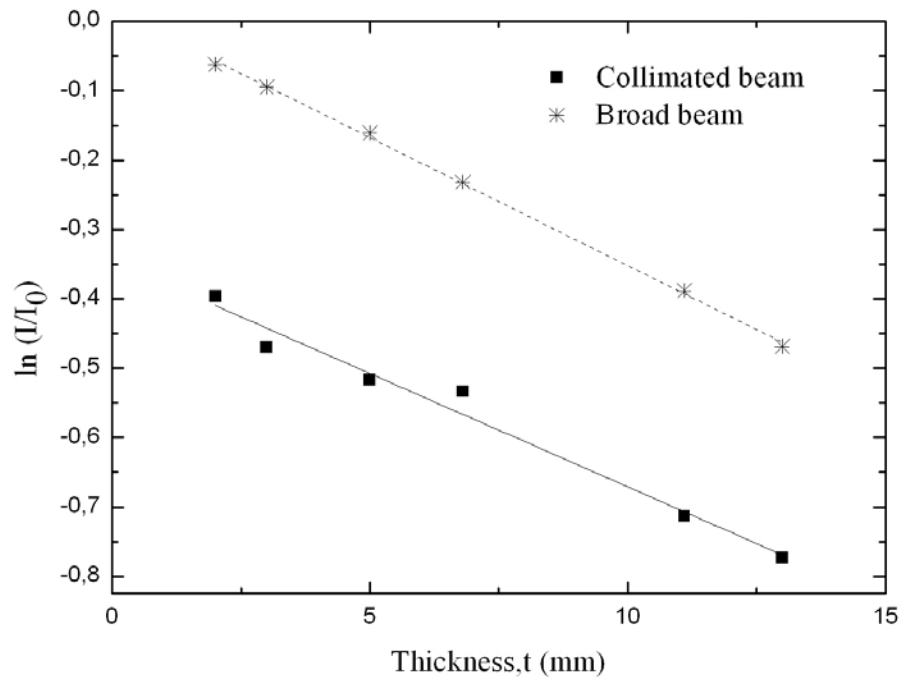
Figure 4.17 Comparison between the intensity in the collimated and broad beam in the ion chamber experiments.
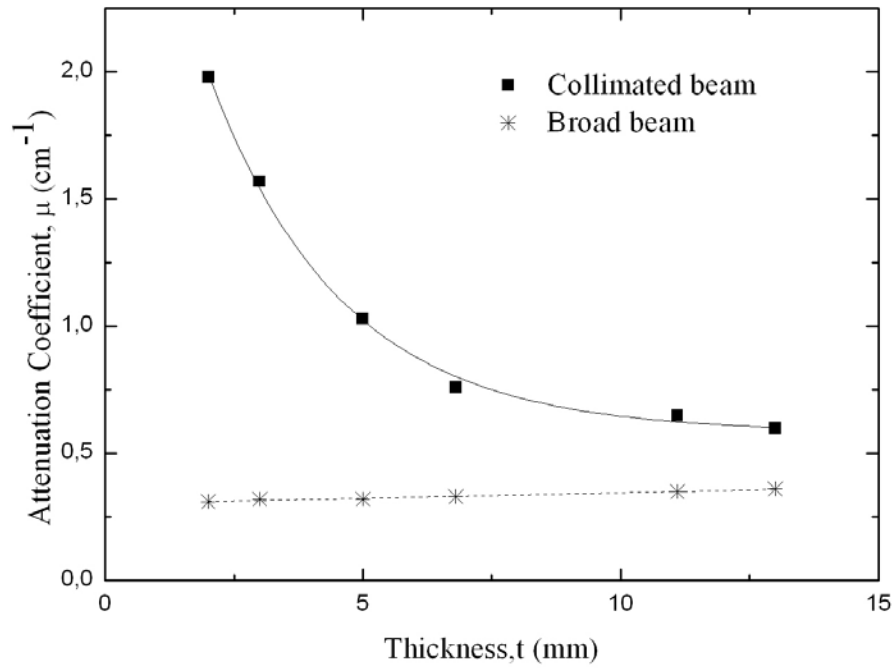
Figure 4.18 Comparison between the attenuation coefficient in the collimated and broad beam in the ion chamber experiments.

CHAPTER 5

CONCLUSION AND FUTURE WORK

In this work, we have calculated the cross sections when the radioisotope Iridium-192 interacts with the carbon steel plates with various thickness using our code that we have developed (refer to Chapter 3). From the calculations, we can conclude that the calculated results are in good agreement with the published results. Hence, our code can be used to calculate incoherent scattering for different materials. We have benchmarked our code for accuracy against the software XCOM obtained from NIST. Our result on the cross section is in good agreement with XCOM, thus, we have extended our code to calculate the linear attenuation coefficient of carbon steel. The calculated effective linear attenuation coefficient carbon steel sample is found to be $0.231 \, \text{cm}^{-1}$. However, the measured effective linear attenuation coefficient of carbon steel (refer to Chapter 4) gives an average value of $0.340 \, \text{cm}^{-1}$. The experimental attenuation coefficient is 32% larger than the theoretical value. In an IAEA 2008 report for the development of protocols for corrosion and deposit evaluation in large diameter steel pipe using radiography, the effective attenuation coefficient was found to be 0.30 cm^{-1} when the source is Cobalt-60 and 0.48 cm^{-1} for Iridium-192 [46]. Thus our experimentally determined effective linear attenuation coefficient of carbon steel is consistent with the literature. From the results, we conclude that the attenuation coefficient calculation especially with regards to the determination of cross section has over estimate the attenuation processes in the sample. In the calculation, the scattering function has been taken into consideration in the Klein-Nishina formula. The actual scattering process is much more complicated and an ab-initio calculation is needed to

determine the value of the attenuation coefficient [47]. Hence, it is important to develop a more comprehensive model for scattering. From this work, it is suggested to calculate the cross sections for every electron in the material, including the inner shell scattering. Considering the dynamic aspects of scattering, the calculations and measurements for first order and second order differential cross sections for total atom scattering and for scattering from electrons of different shells is essential [48]. The impulse approximation in calculating the incoherent scattering should also be considered [49]. From this work, we suggest to use the incoherent scattering functions as proposed by Yalcin [50]. It is also suggested that Monte Carlo method is the best treatment for this calculation.

We have done the calculations on attenuation coefficient using various detectors including film (refer to Chapter 4). We have noticed of the possibility that the variations of grains sizes in films would affect the results in the measurements. This constitutes a limitation of using film for attenuation measurement. We proposed that in measuring the linear attenuation coefficient, the grain size must be taken into consideration.

For future work, various different types of films must be considered; fine, intermediate and coarse grains with each set with different manufacturers for example, Agfa, Kodak and Fuji. One can study on how to quantify density with intensity with regards to grain density. In the research, the intrinsic property of the film must be studied. We would also suggest the treatment using refractive index for calculating the attenuation coefficient [24].

From the results, it is recommended that radiography using films is not suitable in calculating the attenuation coefficient. This is due to the difficulties in getting reliable results when using films. Hence we conclude that the films in radiography technique are

only suitable for visualisation and qualitative examination, for instance in inspecting flaws in certain materials.